



**AFRL-RX-WP-JA-2017-0211**

**ANGLE-BEAM SHEAR WAVE SCATTERING FROM  
BURIED CRACK-LIKE DEFECTS IN BONDED  
SPECIMENS (POSTPRINT)**

**Carson T. Maki, Jennifer E. Michaels, Yu Weng, and Thomas E. Michaels**

**Georgia Institute of Technology**

**19 September 2016  
Interim Report**

**Distribution Statement A.  
Approved for public release: distribution unlimited.**

**© 2017 AIP PUBLISHING LLC**

**(STINFO COPY)**

**AIR FORCE RESEARCH LABORATORY  
MATERIALS AND MANUFACTURING DIRECTORATE  
WRIGHT-PATTERSON AIR FORCE BASE, OH 45433-7750  
AIR FORCE MATERIEL COMMAND  
UNITED STATES AIR FORCE**

REPORT DOCUMENTATION PAGE				Form Approved OMB No. 0704-0188	
<p>The public reporting burden for this collection of information is estimated to average 1 hour per response, including the time for reviewing instructions, searching existing data sources, gathering and maintaining the data needed, and completing and reviewing the collection of information. Send comments regarding this burden estimate or any other aspect of this collection of information, including suggestions for reducing this burden, to Department of Defense, Washington Headquarters Services, Directorate for Information Operations and Reports (0704-0188), 1215 Jefferson Davis Highway, Suite 1204, Arlington, VA 22202-4302. Respondents should be aware that notwithstanding any other provision of law, no person shall be subject to any penalty for failing to comply with a collection of information if it does not display a currently valid OMB control number. <b>PLEASE DO NOT RETURN YOUR FORM TO THE ABOVE ADDRESS.</b></p>					
1. REPORT DATE (DD-MM-YY) 19 September 2016		2. REPORT TYPE Interim		3. DATES COVERED (From - To) 3 March 2014 – 119 August 2016	
4. TITLE AND SUBTITLE ANGLE-BEAM SHEAR WAVE SCATTERING FROM BURIED CRACK-LIKE DEFECTS IN BONDED SPECIMENS (POSTPRINT)				5a. CONTRACT NUMBER FA8650-10-D-5210-0014	
				5b. GRANT NUMBER	
				5c. PROGRAM ELEMENT NUMBER	
6. AUTHOR(S) Carson T. Maki, Jennifer E. Michaels, Yu Weng, and Thomas E. Michaels – Georgia Institute of Technology				5d. PROJECT NUMBER	
				5e. TASK NUMBER 0014	
				5f. WORK UNIT NUMBER X0GQ	
7. PERFORMING ORGANIZATION NAME(S) AND ADDRESS(ES) Georgia Institute of Technology, 311 Ferst Dr, Atlanta, GA 30332				8. PERFORMING ORGANIZATION REPORT NUMBER	
9. SPONSORING/MONITORING AGENCY NAME(S) AND ADDRESS(ES)  Air Force Research Laboratory Materials and Manufacturing Directorate Wright-Patterson Air Force Base, OH 45433-7750 Air Force Materiel Command United States Air Force				10. SPONSORING/MONITORING AGENCY ACRONYM(S) AFRL/RXCA	
				11. SPONSORING/MONITORING AGENCY REPORT NUMBER(S) AFRL-RX-WP-JA-2017-0211	
12. DISTRIBUTION/AVAILABILITY STATEMENT Distribution Statement A. Approved for public release: distribution unlimited.					
13. SUPPLEMENTARY NOTES PA Case Number: 88ABW-2016-4606; Clearance Date: 19 Sep 2016. This document contains color. Journal article published in AIP Conference Proceedings, Vol. 1806, Feb 2017. © 2017 AIP Publishing LLC. The U.S. Government is joint author of the work and has the right to use, modify, reproduce, release, perform, display, or disclose the work. The final publication is available at <a href="http://dx.doi.org/10.1063/1.4974544">http://dx.doi.org/10.1063/1.4974544</a>					
14. ABSTRACT (Maximum 200 words) Ultrasonic wavefield imaging, which refers to the measurement of wave motion on a 2-D rectilinear grid resulting from a fixed source, has been previously applied to angle-beam shear wave propagation in simple plates with through-holes and far-surface notches. In this prior work, scattered waves were analyzed using baseline subtraction of wavefields acquired before and after a notch was introduced. In practice, however, defects of interest often occur between bonded layers and it is generally not possible to record data from the same specimen in both the undamaged and damaged states, even in the laboratory. Direct baseline subtraction of wavefields thus becomes impractical as a tool for analyzing scattering. This present work considers measurement and analysis of angle-beam waves in bonded specimens with and without buried defects originating from fastener holes. Data from fastener holes with and without simulated damage in the form of notches are compared, and it is shown that wavefield baseline subtraction, even after correcting for misalignment between scans, is ineffective for isolating scattering from the notch. A combination of frequency-wavenumber filtering and spatial windowing is proposed and implemented as an alternative approach to quantify scattering from damage.					
15. SUBJECT TERMS Backscattering . Ultrasonography . Spatial filtering . Ultrasonic scattering . Scattering measurement					
16. SECURITY CLASSIFICATION OF:			17. LIMITATION OF ABSTRACT: SAR	18. NUMBER OF PAGES 12	19a. NAME OF RESPONSIBLE PERSON (Monitor) Eric Lindgren 19b. TELEPHONE NUMBER (Include Area Code) (937) 255-9806
a. REPORT Unclassified	b. ABSTRACT Unclassified	c. THIS PAGE Unclassified			

# Angle-Beam Shear Wave Scattering from Buried Crack-like Defects in Bonded Specimens



Carson T. Maki<sup>1,a)</sup>, Jennifer E. Michaels<sup>2,b)</sup>, Yu Weng<sup>2)</sup>, and Thomas E. Michaels<sup>2)</sup>

<sup>1</sup> Woodruff School of Mechanical Engineering, Georgia Institute of Technology, Atlanta, GA 30332-0405

<sup>2</sup> School of Electrical and Computer Engineering, Georgia Institute of Technology, Atlanta, GA 30332-0250

<sup>a)</sup> carson.maki@gatech.edu

<sup>b)</sup> corresponding author: jemichaels@gatech.edu

**Abstract.** Ultrasonic wavefield imaging, which refers to the measurement of wave motion on a 2-D rectilinear grid resulting from a fixed source, has been previously applied to angle-beam shear wave propagation in simple plates with through-holes and far-surface notches. In this prior work, scattered waves were analyzed using baseline subtraction of wavefields acquired before and after a notch was introduced. In practice, however, defects of interest often occur between bonded layers and it is generally not possible to record data from the same specimen in both the undamaged and damaged states, even in the laboratory. Direct baseline subtraction of wavefields thus becomes impractical as a tool for analyzing scattering. This present work considers measurement and analysis of angle-beam waves in bonded specimens with and without buried defects originating from fastener holes. Data from fastener holes with and without simulated damage in the form of notches are compared, and it is shown that wavefield baseline subtraction, even after correcting for misalignment between scans, is ineffective for isolating scattering from the notch. A combination of frequency-wavenumber filtering and spatial windowing is proposed and implemented as an alternative approach to quantify scattering from damage. Despite unavoidable deviations from specimen-to-specimen caused by factors such as variations in bonding, transducer mounting, and fastener hole machining, it is shown that scattering from buried notches can be clearly visualized in recorded wavefield data of bonded plates containing a buried defect as opposed to “baseline” wavefield data taken from a nominally similar specimen with no defect present. Backscattering is further quantified in the form of scattering patterns at different scattering frames to quantify the effect of the notch on the total backscattered wavefield.

## INTRODUCTION

Ultrasonic nondestructive evaluation (NDE), which uses high-frequency acoustic waves to evaluate materials without compromising their integrity, refers to a family of techniques that are frequently applied for detecting and characterizing defects in aerospace materials [1]. Because of its potential for high-fidelity defect detection in a variety of applications, ultrasonic NDE research has largely focused on ultrasonic wave scattering from defects: such as understanding the scattering behavior of fatigue cracks emanating from fastener holes in aluminum structural components [2].

Angle-beam ultrasonic NDE uses an angled wedge to inject bulk waves into the material, which is particularly useful for far-surface defect interrogation. Ultrasonic NDE techniques using angle-beam wedges coupled to PZT transducers have also been utilized in measuring the depth of surface-breaking cracks [3] and for in situ sizing of fastener hole cracks [2]. Both of these studies focused on defect characterization whereas the scattered wavefield itself has also been of interest; Zhang *et al.* investigated the effect of crack roughness on defect scattering for longitudinal bulk waves [4] and Kummer *et al.* considered the effect of various fastener hole fill conditions on shear wave scattering [5]. However, these works were limited to unbonded single plate specimens. Feasibility studies on evaluating aluminum-aluminum bonded specimens using ultrasonic NDE have been discussed [6], but there exists little experimental data reported on bulk wavefield scattering in bonded plates with fastener holes. Instead, much of the reported research on angle-beam ultrasonic NDE considers analytical models with simple defect geometries.

It is important to detect and characterize buried defects emanating from through-holes in bonded plate-like structures for aerospace applications. The depth of the buried defect may be much greater than the size of the defect itself; the relatively small size of defects of interest necessitates high-frequency ultrasound for detection whereas the defect’s corresponding depth renders guided wave methods [7,8] less useful. Ultrasonic wavefield imaging combined with signal processing can be applied to angle-beam shear waves propagating in simple plates with

through-holes and far-surface notches to characterize the scattered wavefield from known defects. Understanding scattering from known defects is important for improving nondestructive evaluation methods that can be applied to characterize cracks emanating from fastener holes. The aim of this work is to develop robust wavefield data analysis techniques for angle-beam ultrasonic NDE and characterize scattering from known crack-like defects emanating from fastener holes.

## EXPERIMENTS

The experimental setup consists of a fabricated bonded specimen that contains one through-hole with a known defect and a second undamaged through-hole. The bonded specimen was sufficiently large compared to the scan area so that edge reflections could be neglected, and the specimen scanning surface was mirror-finished to maximize the signal-to-noise ratio for the recorded laser Doppler vibrometer (LDV) signals.

The specimen was fabricated from two mirror-finished 6061 aluminum plates bonded together using degassed EA E-120HP Loctite epoxy. The bonded specimen dimensions were  $280 \text{ mm} \times 280 \text{ mm} \times 9.53 \text{ mm}$  with three holes of 6.35 mm diameter drilled into the specimen: two undamaged through-holes and one with a 3 mm-long,  $45^\circ$  corner notch emanating from a through-hole on the far-surface of the “top” (i.e. scanning surface) plate. Figure 1 shows sketches of the top view of the plate.

As shown in the side view of the specimen via Fig. 2, angle-beam shear waves were generated using a 5 MHz, 6.35 mm diameter Olympus transducer excited with a Panametrics 5072PR pulser-receiver (impulsive excitation). Wavefield sensing was conducted using a Polytec LDV mounted on an XYZ scanner. As shown in Fig. 2, the transducer was placed 1.5 skips (three path lengths) away from the notch-through-hole intersection. It was then aligned along the x-axis to ensure maximal backscattering from the notch-hole corner in pulse-echo mode.

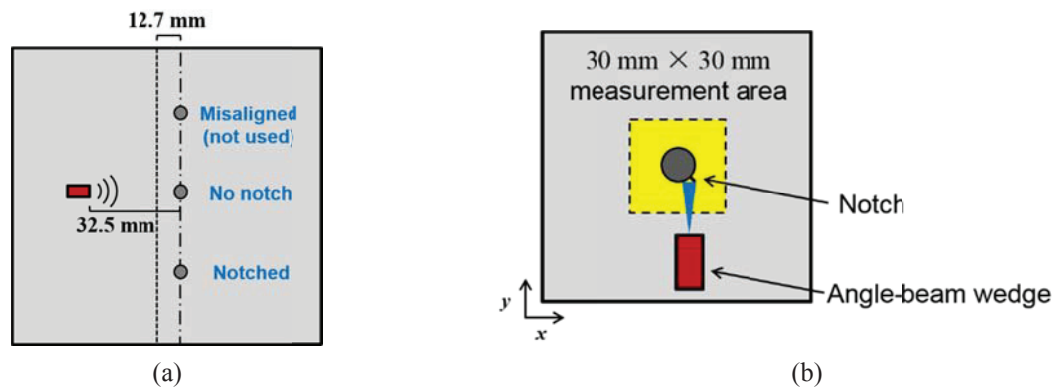


**FIGURE 1.** (a) Top view of the specimen and transducer, and (b) illustration of the scan area for the notched through-hole.

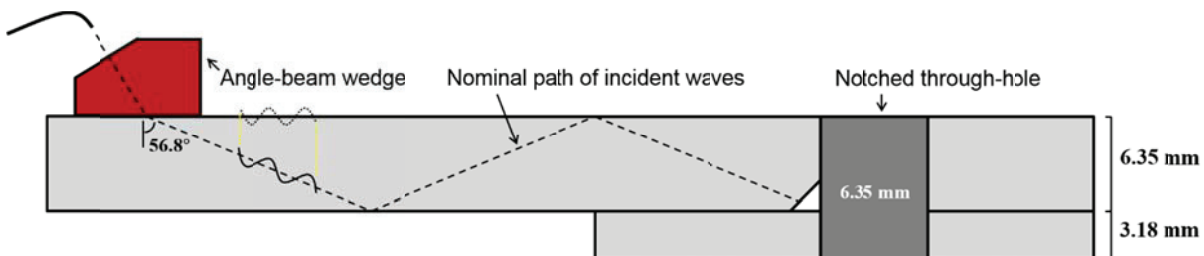


**FIGURE 2.** Side-view of angle-beam bulk wave propagation through the bonded specimen detailing the projected wavelength at the sensing surface.

The two 6061 aluminum plates comprising the bonded specimen were riveted together, and three 6.35 mm through-holes were drilled along a line located  $\sim 165$  mm from one edge of the plates. The “bottom” 3.175 mm plate was bisected at 127 mm from the same reference edge, ensuring that 12.7 mm of the bottom plate was accessible to propagating bulk waves before the through-hole. The bottom plate bisection was done to ensure that the first skip occurred at the aluminum-air boundary to minimize energy leakage into the bottom layer. This is important for ensuring that the majority of shear wave energy interacts with the buried notch at the far-surface of the top plate.

## SIGNAL PROCESSING

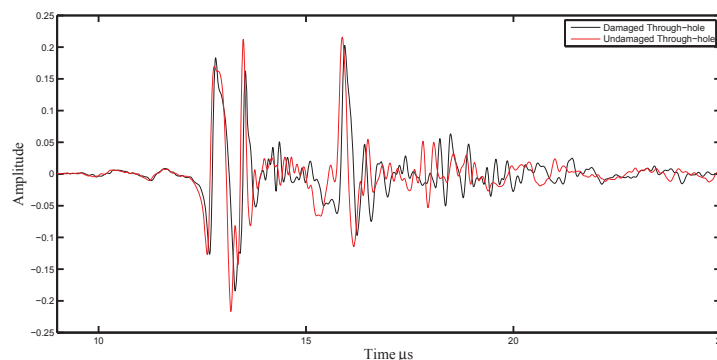
Figure 3 shows typical waveforms from both the damaged and undamaged holes; these signals were recorded at  $x = 5.0$  mm,  $y = -26.0$  mm relative to the center of the through-hole. The signal from the undamaged hole consists of backscattered and mode-converted echoes from the through hole, and contains shear, longitudinal and Rayleigh wave components. The signal from the damaged hole, which is a compound scatterer composed of both the through-hole and the notch, includes additional echoes backscattered from the notch. Several signal processing techniques were applied to separate the defect (notch) scattering from the rest of the wavefield.

### Wavefield Baseline Subtraction

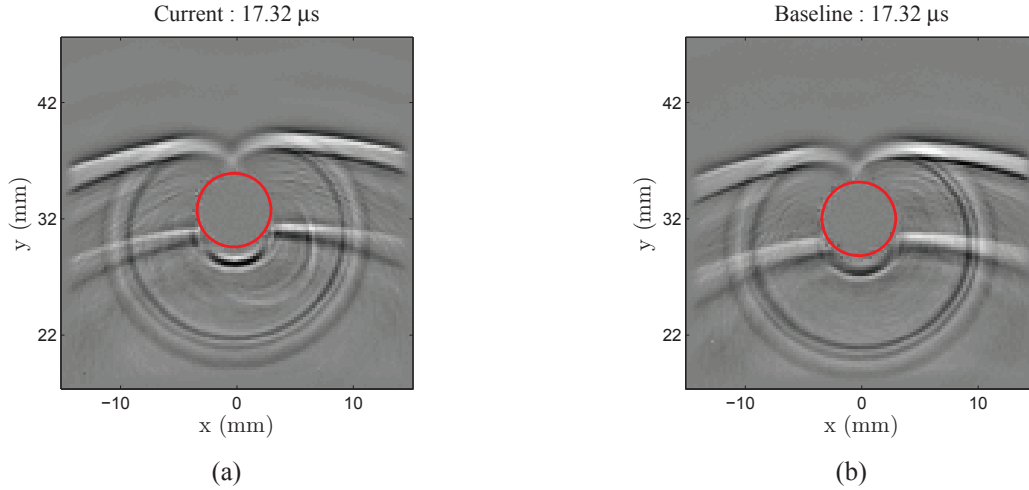
Wavefield baseline subtraction (WBS), as its name implies, consists of subtracting two similar wavefields to isolate the differences between them. As previously implemented in [10], WBS was used in conjunction with spatial and temporal alignment of the baseline data. The alignment makes WBS more robust by handling small discrepancies in current and baseline wavefield alignment.

Figure 4 shows wavefield frames at  $17.32 \mu\text{s}$  of both the damaged and undamaged through-holes. Clear scattering from the notch can be visualized easily in the time-space (T-S) domain in Fig. 4(a) as compared to the frame of Fig. 4(b) from the undamaged hole. Figure 5(a) shows the corresponding residual frame after direct WBS without any alignment, and Fig. 5(b) shows the optimal residual frame after aligning the baseline wavefield from the undamaged through-hole to that of the damaged through-hole. Direct subtraction completely fails to isolate the notch-scattered waves from the total wavefield. Baseline alignment does improve the ability of WBS to reduce the incident waves, but the hole-scattered waves are still quite large in amplitude.

The primary reason that WBS fails is that unlike the results reported in [10], the baseline data from the undamaged hole were recorded from a different through-hole than the notched hole data. The specimen fabrication procedure required that the notch be introduced prior to bonding the second plate to the first, resulting in a “buried” defect. Thus the baseline wavefield data had to be acquired from an undamaged through-hole different from the notched through-hole. The alignment algorithm was previously shown to be effective for global repositioning of the plate in between subsequent scans [10], but that was only one possible variation for the data shown here. Not only was a global shift in the plate possible, it was also likely that the transducer position relative to the through-hole was not identical for the two scans. Given that the shear wavelength at 5 MHz is  $\sim 0.5$  mm, even small offsets in transducer placement will yield significant changes in the resulting wavefield. These changes, combined with unavoidable variations in coupling and machining, result in WBS failing to isolate the notch-scattered waves.



**FIGURE 3.** Typical LDV signals recorded from both the damaged and undamaged holes.



**FIGURE 4.** (a) “Current” area scan of the damaged fastener hole (b) “Baseline” area scan of the undamaged fastener hole.

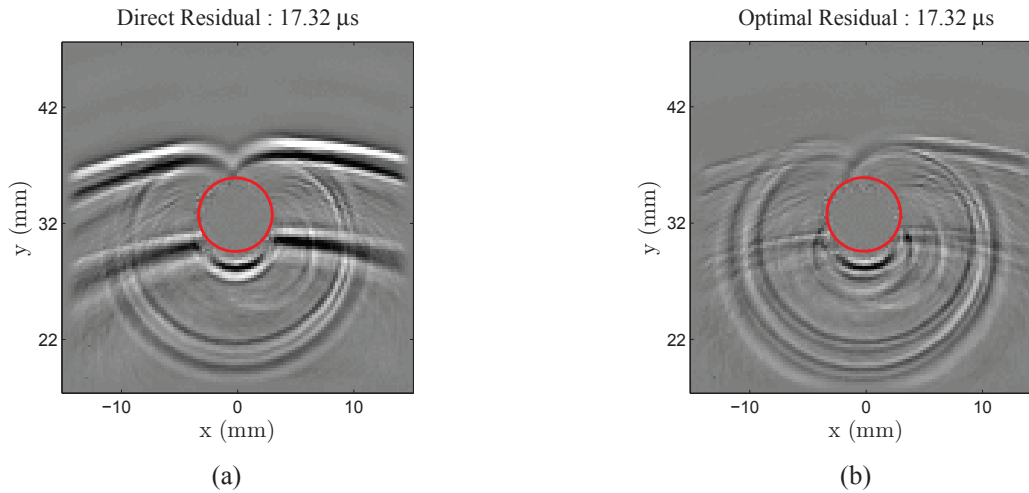


**FIGURE 5.** (a) Direct residual obtained by subtraction of the baseline wavefield from the current wavefield. (b) Residual after spatial alignment of the baseline wavefield.

## Wavefield Filtering

Because WBS fails to separate the defect scattering from the through-hole scattering, alternative signal processing techniques are applied. As can be seen in Fig. 4(a), the scattering from the notch does not spatially overlap with the through-hole scattering for this particular scattering frame. However, there are situations in which the notch scattering is much more overlapped with the through-hole scattering. These situations generally indicate that the transducer is not properly located relative to the hole and the notch, and are not further considered here. However, in many NDE applications the exciting transducer is located so that the scattered wavefield from the defect of interest (the notch) can be separated from scattering from benign structural elements (the through-hole). In this section a two-step wavefield filtering procedure is described that facilitates this separation.

### Phase Velocity Filtering

Fourier domain frequency-wavenumber filtering is used to separate the shear wave mode from the full wavefield by phase velocity ( $c_p$ ) and to remove forward propagating ( $+k_y$ ) waves. The  $c_p$  filter works by first applying a 3-D Fourier transform to the wavefield:

$$w(t, x, y) \rightarrow W(\omega, k_x, k_y) . \quad (1)$$

The resulting Fourier-domain data are sorted into three  $c_p$  ranges as given in Table 1.

**Table 1.** Phase velocity ranges for frequency-wavenumber filtering.

Mode	Phase Velocity Range (mm/ $\mu$ s)
Rayleigh	2.4 – 3
Shear	3 – 6.4
Longitudinal	6.4 – 12.8

The phase velocity ranges are determined by considering  $k_x$ - $k_y$  slices in the frequency-wavenumber domain [12]. Keeping in mind that frequency, wavenumber, and phase velocity are related via

$$k = \frac{\omega}{c_p} , \quad (2)$$

it is straightforward to construct basic phase velocity filters capable of sorting the wavefield by wave modes in the Fourier domain. However, a geometric transformation is required to obtain the true phase velocity for the shear and longitudinal modes because the apparent wavelength is projected onto the surface of the plate and is not the same as the wavelength along the direction of bulk wave propagation. As is illustrated in Fig. 2, the apparent wavelength on the surface is smaller than that in the bulk material, and the phase velocity is correspondingly larger.

$$c_p = \frac{c}{\sin \theta_r} . \quad (3)$$

Equation (3) gives the phase velocity measured on the surface of the plate as a function of the refracted angle,  $\theta_r$ , and the bulk wave speed,  $c$  [11]. Since the denominator is bounded by 0 and 1, there is ambiguity between small-refracted angle shear waves and large-refracted angle longitudinal waves. Therefore, keep in mind that small-refracted-angle shear waves may be excluded from the shear mode wavefield and instead are mixed with the longitudinal mode wavefield post  $c_p$  filtering.

### Wavenumber Filtering

Positive wavenumber filtering is done by applying a Gaussian filter to  $W(\omega, k_x, k_y)$ . The incident and forward scattered waves, which correspond to  $+k_y$ , are removed from the wavefield to focus on and limit further processing to backscattered waves. The  $+k_y$  waves are removed because the backscattered waves are of more interest for NDE. Filtering out the  $+k_y$  waves allows detailed analysis of backward scattered waves to better visualize and characterize notch scattering.

Figure 6(a) shows the 17.32  $\mu$ s frame of the damaged through-hole after phase velocity filtering is used to extract only shear waves. Figure 6(b) is the corresponding frame of shear waves after applying the  $+k_y$  filter. Note that the cutoff occurs at  $\pm 84.4^\circ$  from the maximum  $+k_y$  value (i.e., due north in the wavefield) as marked with two yellow lines in Fig. 6(b). The cutoff is located so that there is a smooth transition between the filter cutoff and the complete backscatter region (i.e.,  $180^\circ \rightarrow 360^\circ$ ).

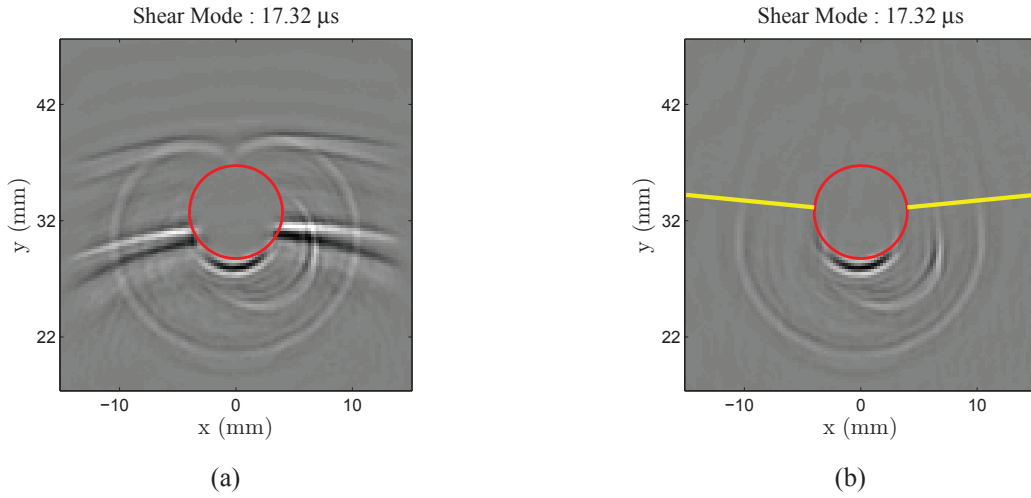


**FIGURE 6.** Frames at  $17.32 \mu\text{s}$  from the notched hole scans. (a) After phase velocity filtering to extract the shear mode, and (b) after  $+k_y$  filtering applied to the extracted shear mode wavefield.

### Notch Characterization

After applying both the  $c_p$  and  $+k_y$  filters, complicated backscattering is more easily visible in the resulting filtered wavefield shown in Fig. 6(b). Because the notch backscattering is spatially displaced from the through-hole backscattering, radial energy calculations relative to the center of the hole can be used to quantify the notch backscattering as a function of the observer direction (polar angle) by integrating along a radial path in the spatial domain at a fixed time.

Figure 7 shows designated radial paths in the spatial domain at a selected frame. For the current work, the radial path length is 3 mm and 181 radial paths are considered to form a semi-circular ring of radial energy calculations covering the backscatter region (i.e.  $180^\circ \rightarrow 360^\circ$ ). The center of the through-hole is designated as the observer reference location with each polar angle corresponding to the observer direction. The final result is a plot of energy versus angle for the backscattered region and specified frame.

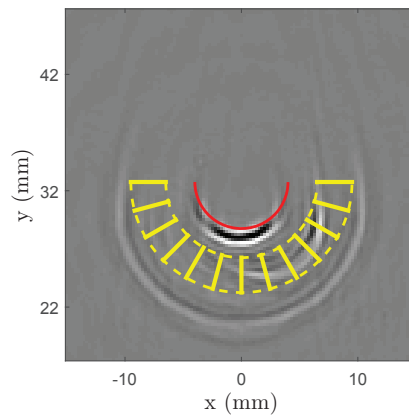


**FIGURE 7.** The semi-circular ring for radial energy calculations, illustrating 13 of the radial lines of 3 mm length.

## Methodology Summary

The complete methodology for segregating the defect element (e.g., a notch) from a compound scatterer (e.g., through-hole + notch) is summarized as follows:

- **Filter wavefield by wave mode.** In the case of angle-beam bulk waves, three modes are present: the surface Rayleigh wave, shear and longitudinal bulk waves. Here, the shear wave mode is of interest and is separated by phase velocity filtering.
- **Isolate backscattering by  $+k_y$  filtering.** For the present work, backscattering was of most interest for detecting and characterizing the defect; however, any general direction of scattering can be separated from the full wavefield by specifying a range of wavenumber values.
- **Calculate and analyze radial energy.** Although it is most important for characterizing the defect scattering, radial energy can provide insight into the scattering behavior of the entire compound scatterer.

## RESULTS AND DISCUSSION

Radial energy was calculated for three scattering frames: 16.32  $\mu\text{s}$ , 17.32  $\mu\text{s}$ , 18.32  $\mu\text{s}$ . Radial energy is used to generate scattering patterns and is plotted in both polar and rectangular presentations. The polar plot helps fortify intuition of the scattering direction while the rectangular plot allows for a more detailed analysis of the exact angle(s) along which the backscattered shear waves are propagating. The same analysis is performed for both damaged (current) and undamaged (baseline) through-hole wavefields. All results are shown in Fig. 8, where each column corresponds to the same frame, and from top-to-bottom are shown frames of the damaged and undamaged through-holes, polar energy plots, and rectangular energy plots respectively.

At 16.32  $\mu\text{s}$ , the current and baseline wavefields appear to be very similar and consist primarily of the weak backscattered first skip from the through-hole; there is no significant scattering visible from the notch. The energy profile of the current wavefield is close to that of the baseline, yet the radial energy in almost all directions is stronger in the current. The reduction in energy is likely due to epoxy residue in the undamaged through-hole, as epoxy filling is shown to decrease the reflection coefficient of incident shear waves scattering from the through-hole. Kummer elaborates on the effect of through-hole fill conditions in isotropic plates in further detail and presents experimental justification for the effect [5].

The frame at 17.32  $\mu\text{s}$  clearly show a notch-scattered wave that reaches its maximum value at an angle of  $332^\circ$  relative to the center of the through-hole. The larger amplitude backscattered second skip from the through-hole is also visible in both the damaged and undamaged through-hole frames. Evidently, the notch-scattered wave visible in this frame has resulted from the first incident skip, but has emerged at a shallower angle than that of the nominal notch orientation ( $-28^\circ$  compared to  $-45^\circ$ ).

The final frame, at 18.32  $\mu\text{s}$ , shows a second backscattered wave from the notch that is partially overlapped with the backscattered second shear skip from the through-hole. This backscattered wave, which appears to result from the second shear incident skip, has its peak amplitude close to  $270^\circ$ , which is the expected direction of the corner echo. The notch-scattered wave overlaps with the backscattered second shear skip from the hole for propagation directions between  $270^\circ$  and  $360^\circ$ , which likely includes both constructive and destructive interference.

These observations are somewhat puzzling because of the inconsistency in timing, directionality, and amplitude between the notch-scattered waves from the two skips. As observed above, the first notch-scattered wave is well-separated from the hole-scattered wave and has its peak at about  $332^\circ$ , whereas the second notch-scattered wave overlaps the hole-scattered wave and the radial energy shows a peak at around  $270^\circ$ . However, the peak at  $270^\circ$  is a combination of the notch and through-hole backscattered waves, so it cannot be directly attributed to notch scattering. Furthermore, this energy “maximum” is misleading because constructive and destructive interference in the  $270^\circ$  to  $360^\circ$  region may obscure the primary scattering direction of the notch-scattered wave from the second skip. In addition, it would be expected that the second incident shear skip, which is at the nominal refracted angle for a back surface reflection, should generate a much stronger backscattered wave than the first skip, which is very shallow. This appears to be the case for the hole backscattering but is difficult to confirm for the notch since it is not sufficiently separated from the hole backscattered wave.

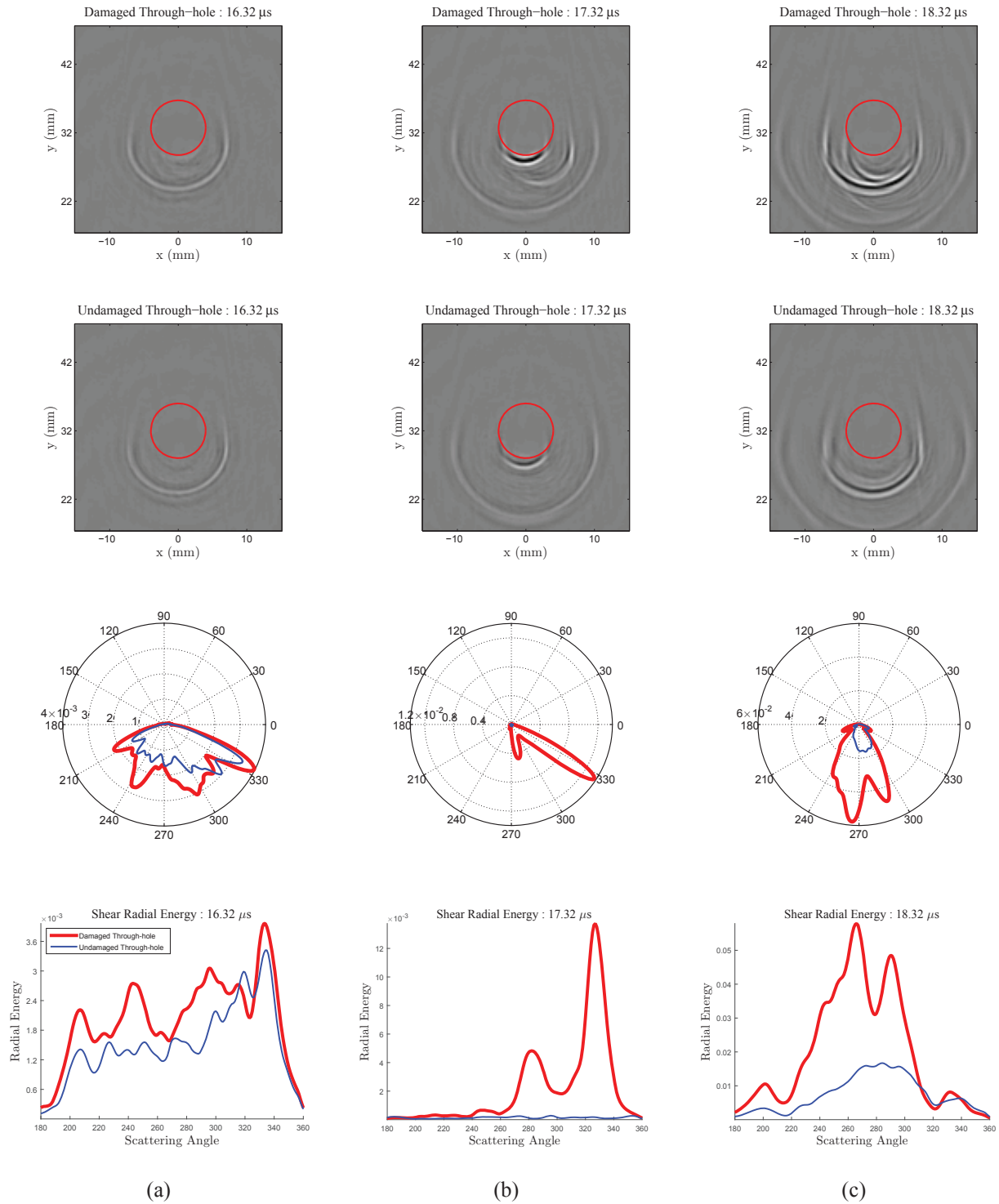


**FIGURE 8.** Scattering results for the following frame times: (a) 16.32  $\mu\text{s}$ , (b) 17.32  $\mu\text{s}$ , and (c) 18.32  $\mu\text{s}$ . From top-to-bottom are shown frames from the damaged through-hole, frames from the undamaged through-hole, polar energy plots, and rectangular energy plots.

The results shown here not only demonstrate a methodology to quantify scattering, but also point out the challenges in interpreting data recorded from complicated specimens with compound scatterers. Although the specimen used here was carefully fabricated, there are undoubtedly variations in machining, transducer mounting, and bond layer uniformity that make interpretation of results even more challenging. Furthermore it is not clear from only front surface measurements whether or not significant energy has penetrated through the epoxy bond into the second layer, which could affect both timing and backscattered energy.

## CONCLUSIONS

The results presented here demonstrate that shear wave scattering from a buried defect emanating from the far surface of a 6.35 mm diameter through-hole of a bonded, multi-layer specimen can be characterized by analyzing the compound backscattering from both the defect and through-hole elements. Filtering the wavefield by phase velocity and wavenumber and analyzing radial energy at multiple scattering frames allows backscattering from the notch to be completely separated from incident waves and better separated from hole-scattered waves. It was further shown that wavefield baseline subtraction is inadequate for separating the defect element scattering from the compound scattering wavefield. For the specimen considered, it was possible to identify a wavefield frame and spatial window for which the notch backscattering could be separated from the hole backscattering. These results demonstrate a methodology for characterizing an element (i.e., the notch) of a compound scatterer (i.e., hole + notch) without using baseline subtraction.

It is noteworthy that the radial energy calculation method is helpful for generating scattering patterns but fails to separate spatially overlapped defect and through-hole backscattering. The energy calculation essentially lumps the different element scattering effects together to get a comprehensive energy representation for each radial path. It also should be kept in mind that since bulk wavefield measurements only capture the out-of-plane motion on the specimen surface, it is not possible to fully understand the internal bulk wavefield. Future work should consider additional measurements on the far side of the specimen as well as a wider variety of specimen geometries, transducer frequencies, and incident angles. It is hoped that future modeling efforts will complement experimental studies, such as the work reported here, to more fully understand the complicated interactions between incident waves and compound scatterers.

## ACKNOWLEDGMENTS

This work is sponsored by the Air Force Research Laboratory, contract number FA8650-10-D-5210, Dr. Eric Lindgren, program manager.

## REFERENCES

1. L. W. Schmerr Jr., *Fundamentals of Ultrasonic Nondestructive Evaluation*, (Springer, Switzerland, 2016).
2. J. E. Michaels, T. E. Michaels, "An ultrasonic angle beam method for in situ sizing for fastener hole cracks," *Journal of Nondestructive Evaluation*, **25**, pp. 3-16 (2006).
3. M. V. Felice, A. Velichko, and P. D. Wilcox "Accurate depth measurement of small surface-breaking cracks using an ultrasonic array post-processing technique," *NDT & E International*, **68**, pp. 105-112 (2014).
4. J. Zhang, B. W. Drinkwater, and P. D. Wilcox "Longitudinal scattering from rough crack-like defects," *IEEE Transactions on Ultrasonics, Ferroelectrics, and Frequency Control*, **62**, pp. 545-559 (2015).
5. J. W. Kummer, A. J. Dawson, J. E. Michaels, and T. E. Michaels "Effect of fill conditions on bulk wave scattering from a through-hole," in *Review of Progress in Quantitative Nondestructive Evaluation*, eds. D. E. Chimenti and L. J. Bond, (American Institute of Physics **1706**, Melville, NY), **35**, 030021-1 to 8 (2016).
6. J. L. Rose, *Ultrasonic Nondestructive Evaluation Technology for Adhesive Bond and Composite Inspection*, (Springer, U.S., 1991).
7. X. Chen, J. E. Michaels, and T. E. Michaels "Incremental scattering of guided waves from a notch originating at a through-hole," in *Review of Progress in Quantitative Nondestructive Evaluation*, eds. D. E. Chimenti and L. J. Bond, (American Institute of Physics **1650**, Melville, NY), **34**, pp. 799-806 (2015).
8. P. Fromme, M. B. Sayir "Detection of cracks at rivet holes using guided waves," *Ultrasonics*, **40** (1), pp. 199-203, 2015.

9. A. J. Dawson, J. E. Michaels, R. M. Levine, X. Chen, and T. E. Michaels, "Acquisition and analysis of angle-beam wavefield data," in *Review of Progress in Quantitative Nondestructive Evaluation*, eds. D. E. Chimenti and L. J. Bond, (American Institute of Physics **1581**, Melville, NY), **33**, pp. 1716-1723, 2014.
10. A. J. Dawson, J. E. Michaels, and T. E. Michaels, "Isolation of ultrasonic scattering by wavefield baseline subtraction," *Mechanical Systems and Signal Processing*, **70-71**, pp. 891-903, 2016.
11. A. J. W. Dawson, *Acquisition and Analysis of Ultrasonic Wavefield Data to Characterize Angle-Beam Propagation and Scattering in Plates*, Ph.D. thesis, Georgia Institute of Technology, 2015.
12. J. W. Kummer, *Signal Processing Methods to Quantify Scattering of Angle-beam Shear Waves from Through-holes in Plates*, M.S. thesis, Georgia Institute of Technology, 2015.